A study of composite material damage induced by laser shock waves

Romain Ecault [a,*], Michel Boustie [a], Fabienne Touchard [a], Frédéric Pons [a], Laurent Berthe [b], Laurence Chocinski-Arnault [a], Bastien Ehrhart [c], Clemens Bockenheimer [d]

[a] Institut PPRIME, CNRS-ENSMA-Université de Poitiers, Département Physique et Mécanique des Matériaux – ENSMA, 1, Av. Clément Ader, B.P. 40109, 86961 Futuroscope Cedex, France
[b] PIMM, CNRS-ENSAM Paristech, 151 Bd de l'Hopital, 75013 PARIS Cedex, France
[c] Fraunhofer Institute for Non-Destructive Test Methods (IZFP), Campus E3.1, 66123 Saarbruecken, Germany
[d] Airbus Operations SAS, Leader SHM & ENDT Technology, A350 Materials & Processes (ESKW), Site de Saint Martin du Touch, 31060 Toulouse Cedex 9, France

A B S T R A C T

A laser shock wave technique has been used to study the damage tolerance of T800/M21 CFRP (Carbon Fiber Reinforced Polymer) composite material with different lay_ups. Different levels of damage have been created according to various laser irradiation conditions. Several characterization methods such as Optical Microscopy, X-ray Radiography, or Interferometric Confocal Microscopy have been used to quantify these defects. The nature of the defects induced by the shock wave propagation has been studied. The sensitivity of the composite material damage to the shock conditions has been shown and quantified. Moreover, the experimental results gathered with each technique have been compared to each other and it leads to a better understanding of the CFRP behavior under high dynamic loading. These original results have enabled the definition of a specific damage criterion for CFRP under dynamic loading. s

Keywords:
A. Layered structures
B. Damage tolerance
B. Delamination
D. Optical microscopy

1. Introduction

Nowadays, composite materials are used in aeronautics for their good mechanical properties and their low weight. Increasing their part in aircraft structures is a compulsory step to achieve a better eco-efficiency. The gain could be important, especially thanks to new assembly technologies as bonding which is meant to replace the current techniques like riveting or bolting [1,2]. These methods are expensive, and are not well-adapted to composite materials since complex machining has to be set up (drilling leading to delamination or fiber breakage) [3–5]. Moreover, the use of the bonding technique would enable a significant weight lightening of the aeronautic structures, which means an aircraft consumption reduction. However, several implementation problems can penalize the bonding process, while manufacturing or during the aircraft lifetime. The bond quality can be weakened by a bad curing cycle, a surface contamination before bonding, etc. [6,7]. Moreover, there is no non-destructive technique currently available to quantify the bonding mechanical resistance. Facing this issue, a European Project has been started in November 2010: ENCOMB (Extended Nondestructive testing for COMposite Bonds). New methods are developed to enable first the characterization of the composite surface state before bonding, and then, the certification of the bonding mechanical quality. One of the developed methods is the laser shock wave technique first developed by Vossen and Gupta [8,9]. This technique can create a short but intense inside tensile loading on bonded materials. If these stresses are well-located into an interface, the bond line resistance can thus be tested. The LASAT technique was developed for many cases, especially for metal assemblies or metal coatings, for which it is now well understood [10]. Under some conditions, this technique has already been successfully used to test different bonding strengths of composite assemblies [11–13]. Nevertheless, more investigations remain necessary in order to optimize the technique and to better understand the associated complex physical phenomena. In particular, the composite material dynamic response to laser shocks has to be understood to develop a technique efficient for any kind of bonded composite assembly [14].

From another point of view, the aeronautical composite structures can be subjected to high energy impacts during their lifetime. Indeed, some external loadings can induce high levels of stress with a high strain rate, such as high velocity impacts of various kinds of projectiles (birds, ice stones, etc.). Under some conditions, the laser shocks induce stress levels comparable to the ones induced by high velocity impact. The laser shock wave technique presented in this paper can also be used as a way to test and damage composite material [14–16].

* Corresponding author. Tel.: +33 549498188.
E-mail addresses: romain.ecault@ensma.fr (R. Ecault), michel.boustie@ensma.fr (M. Boustie), fabienne.touchard@ensma.fr (F. Touchard), frederic.pons@ensma.fr (F. Pons), lberthe@gmail.com (L. Berthe), laurence.chocinski@ensma.fr (L. Chocinski-Arnault), bastien.ehrhart@airbus.com (B. Ehrhart), clemens.bockenheimer@airbus.com (C. Bockenheimer).

In both case, a first step is to study the dynamic response of the composite material, which is key information for the applications presented. The laser shocks are used as a laboratory tool able to produce different levels of damage inside the composite material. This technique differs from others as drop weight systems. They are used to produce impacts on composite samples at low energy and long solicitation duration compared to what can be done using a laser shock setup. In case of classic impact loading on CFRP composite, multi delamination and transverse cracks can be observed under the loading area. The propagation of the delaminations mainly depends on the stacking sequence [17–20]. Many numerical models are developed to restitute the composite behavior in these cases of loading. The recent damage models are able to simulate the delamination propagation and the ply cracks initiation and propagation. The 3D models results are useful to understand the dynamic behavior of the composite by comparing simulation and experimental results [21–25]. In this study, laser shocks have been performed on CFRP T800/M21 composite materials. Several diagnostics providing complementary information have been tested to analyze the damage extent and nature resulting from the laser shock wave propagation. Especially, the use of Interferometric confocal microscopy has been extended to the shock composite sample in order to quantify their residual deformation. With these post-shock test methods, the main features of these defects have been obtained: location, anisotropy, main dimensions. The laser shock wave technique has been used as a characterization method to establish the damage threshold of the CFRP composite material tested and the experimental data gathered could provide useful information to optimize numerical modeling results.

2. Material investigated

A T800/M21 (Hexcel) composite material has been used in this investigation. It is well-known as a classic composite material for aeronautical applications, more specifically for structures which are prone to impacts. It is made of a non-conventional matrix, mixed from a thermoset epoxy resin and thermoplastic nodules whose mechanical behavior should enhance the global composite shock resistance. On the tested samples, this composition has been checked using DSC (Differential Scanning Calorimetry) characterization. The glass transition of the epoxy was evaluated around 194 °C and the thermoplastic phase has been identified from the endothermic melting peak close to 212 °C. Micrographs of a 6 mm thick T800/M21 sample are presented in Fig. 1a–c with three different magnifications. This sample is made of 33 pre-impregnated plies assembled with different orientations $[45°/0°/0°/-45°/0°/0°/45°/0°/0°/-45°/0°/-45°/0°/0°/45°/0°/0°_{0.5}]_S$ and cured by autoclave.

On Fig. 1, the thermoplastic nodules can be observed mostly between the plies as round dark grey shapes, but are sometimes present inside the plies, forming channels or veins (see Fig. 1a and b). Their approximated diameter has been evaluated in the range [10–20 μm] (see Fig. 1c). The pre-impregnated plies are about 180 μm, but the presence of the thermoplastic nodules induces a strong deviation of the ply thickness. This 6 mm thick T800/M21 material has provided all the samples tested in this study.

3. The laser shock wave technique

The laser shock wave technique consists in a high power laser irradiation of a target. When focused on a material, this irradiation results in plasma sublimation on its surface. The plasma expanses rapidly, which induces a shock wave into the material by reaction. The shock wave is then propagating through the thickness toward the target back face, according to properties depending on the material characteristics. Reaching the sample back face, the reflection of this shock wave creates a release wave propagating backward. This release wave is crossing the incident unloading wave coming from the front face and initiated by the end of the loading (see in Fig. 2). It is the crossing of these two release waves which can lead to a local high tension area which could damage the material if the stress level is high enough compared to its damage threshold. In fact, the tensile stress level is directly linked to the laser shock amplitude whereas its location mainly depends on the material properties and the pulse characteristics. In order to amplify the pressure level on the sample, a water confinement has been used to enhance the plasma expansion effect [26]. Therefore, the damage initiation for a given material can be controlled by changing the laser source parameters, especially the energy level for the stress intensity, and the pulse duration for the position of this stress area.

All the samples have been coated with aluminum painting before laser irradiation in order to produce a more controlled shock loading. Indeed, if the laser interaction with the aluminum has already been deeply investigated, very few investigations have been conducted on the laser interaction on composite materials [27–30]. Consequently, the correlation between the laser intensity and the corresponding pressure loading on the sample front face is well documented for aluminum.

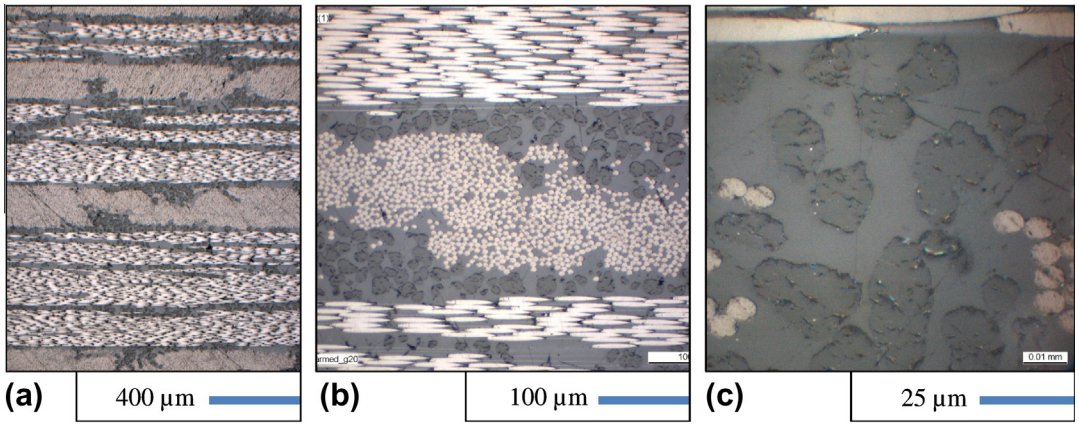

Fig. 1. Optical micrographs (a–c) of a 6 mm thick T800/M21 sample. (For interpretation of the references to color in this figure legend, the reader is referred to the web version of this article).

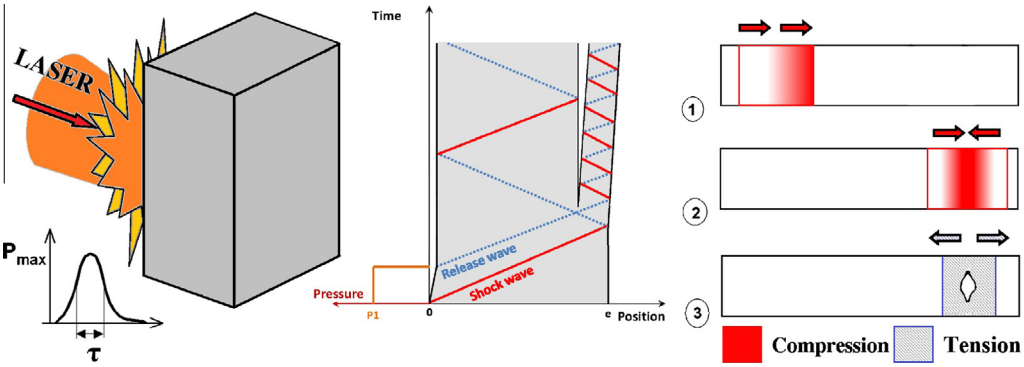

Fig. 2. Sketch of the laser shock damaging technique principle in case of a damage creation. (For interpretation of the references to color in this figure legend, the reader is referred to the web version of this article).

4. Post-shock diagnostics and observations

4.1. Experimental methods

The conditioned samples are first shocked with different laser energy levels to produce different levels of inside damage. Samples are then recovered from the laser experimental setup to be analyzed with several diagnostic setups. A first series of shocks has been performed on 1.5 mm thick T800/M21 samples extracted by cutting out from the thicker material presented in Fig. 1. These samples have been observed using optical micrography to analyze the damage resulting from the laser shock wave propagation. It helped to establish a correlation between the damage main characteristics and the laser intensity. Another laser shock series was performed on 6 mm thick sample presented in Fig. 1. The resulting damage was observed using X-ray radiography and Interferometric Confocal Microscopy (ICM) on the sample back face (opposite to the shocked one). The data gathered was used to evaluate the damage threshold of the T800/M21 CFRP tested under laser shock dynamic loading.

4.2. Thin CFRP sample experiments

Results obtained on 1.5 mm T800/M21 composite samples are presented in this section. These samples were shocked with four different laser energy levels on their front face. The samples have been cut perpendicularly to the 0° fiber direction, and coated in a specific resin to be observed. Results show that the damage induced by the laser shock is cone-shaped through the thickness of the sample, with the cone basis on the back face (see in Fig. 3). This observation is consistent with other scientific work and different impact loadings such as drop tower [14–20]. The same kind of damage can be observed for each laser shock. It can be divided into type groups which are detailed in Table 1. The position numbers given in the first column of Table 1 are referring to the corresponding damage in Fig. 3. The laser spot diameter of 4 mm is also reported on this figure.

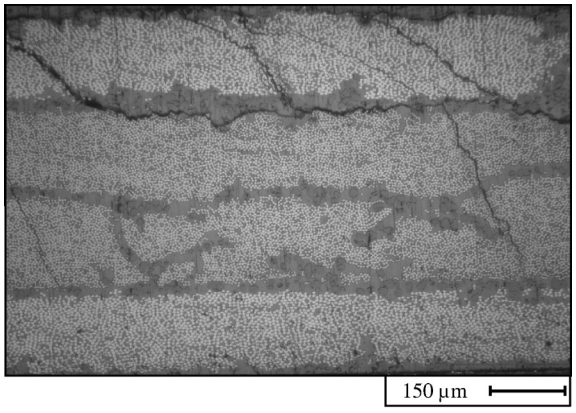

Fig. 4. Close observation of damage resulting from laser shock waves propagation (water confined laser pulse: $I = 5.30$ GW/cm^2, $\Delta t = 30$ ns, $D_{spot} = 4$ mm) – optical micrograph.

Two main types of damage can be observed in a laser shocked composite sample. Transverse cracks in the matrix, through the ply thicknesses can be observed in Fig. 3 and the most obvious damage is delamination between the plies, which can lead to ply ejection if the stresses level is high enough. The delaminations are initiated by the high tensile stresses generated by the propagation of the laser induced shock wave inside the composite. In these experiments, the high power laser irradiation of the composite sample results in a strong pressure load driven on a small spot (4 mm diameter circle) compared to the size of the sample. This induces bending and shear loadings, especially on the side of the impacted area. These high stresses lead to the apparition of transverse cracks perpendicularly to the ply plan inside the composite sample (see in Fig. 3 reference 1 and 5).

An overview of the classic composite damage resulting from laser shock wave propagation is given in Fig. 4. The observed zone is

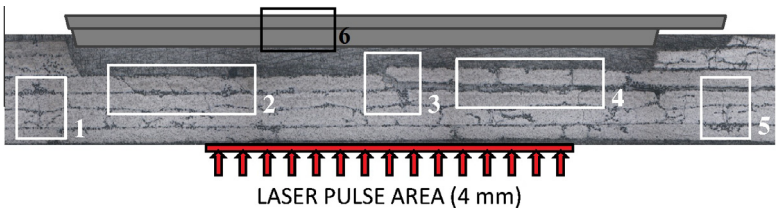

Fig. 3. Damaged composite sample with reference number for damage analysis (water confined laser pulse: $I = 5.30$ GW/cm^2, $\Delta t = 30$ ns, $D_{spot} = 4$ mm) – Optical micrograph. (For interpretation of the references to color in this figure legend, the reader is referred to the web version of this article).

Table 1
List of the common damage observed.

Damage number	Short description of the observed damage
1 and 5	Transverse cracks through several plies close to a zone of high thermoplastic nodule concentration. Located on the edges of the loaded area
2	Local delamination with transverse cracks through the considered ply
3	Important damage with both ply failure and delamination, observed close to a zone of high thermoplastic nodule concentration
4	Two kinds of delamination 1. Delamination with a ply ejection on the back face side. The delamination geometric profile can be observed 2. Delamination without full ply ejection. Observation of the inter-ply after laser shock impact
6	Ejected plies

located under the impact loading area (reference number 2 in Table 1 and Fig. 3). A ply delamination can clearly be identified, as well as transverse cracks inside the top ply. The cracks inside the ply have propagated between the fibers. According to other scientific works, these cracks through the plies are prior to the cracks leading to delamination. In the laser case treated in this paper, it can be assumed too as the high tensile stress area is propagating from the back face to the front face (from top to bottom in Fig. 4). So the plies are loaded before the inter-plies and can be damaged first. The plies that were just above the damaged one have been ejected during the laser shock test due to the high level of tensile stress (see in Figs. 3 and 4). As the tensile loading level is progressively softened because of the energy dissipation resulting from the previous delaminations, the stresses were not strong enough to eject this ply but high enough to damage it.

The profile of the crack leading to delamination can be linked to the presence of thermoplastic nodules inside the composite matrix M21. Indeed, the crack is following the ply surface geometry meanwhile it goes around the thermoplastic nodules. Moreover, cracks going through the nodules have never been observed on the many shocked samples analyzed. Two hypotheses can be made: the first one complies with the main goal of these nodules which is to enhance the shock resistance of composite material. Their presence makes the crack propagation harder because it is increasing the distance to cover before leading to delamination. The second one relies on the fact that adding nodules inside the matrix content

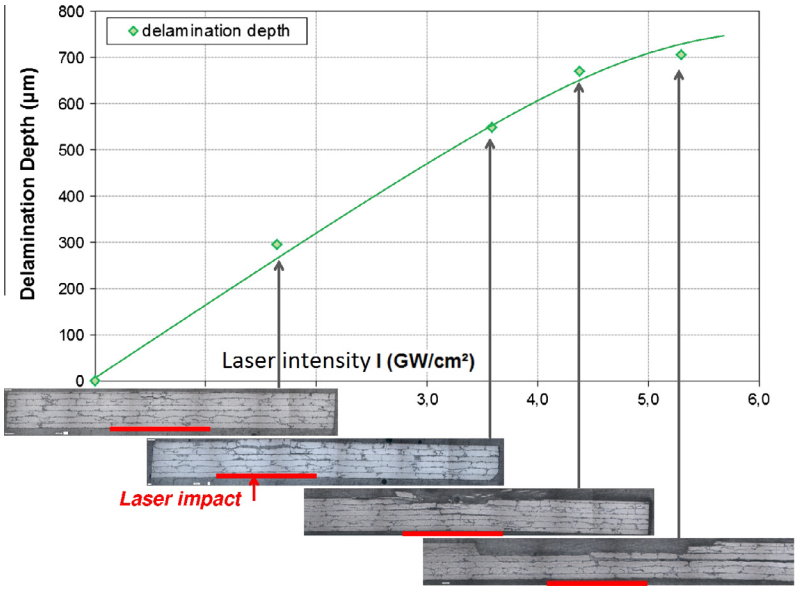

Fig. 5a. Correlation between the laser intensity and the damage depth inside the composite target with the associated micrographies (results obtained by optical inspection of four laser shocks on T800/M21 CFRP target, 1.5 mm thick). (For interpretation of the references to color in this figure legend, the reader is referred to the web version of this article).

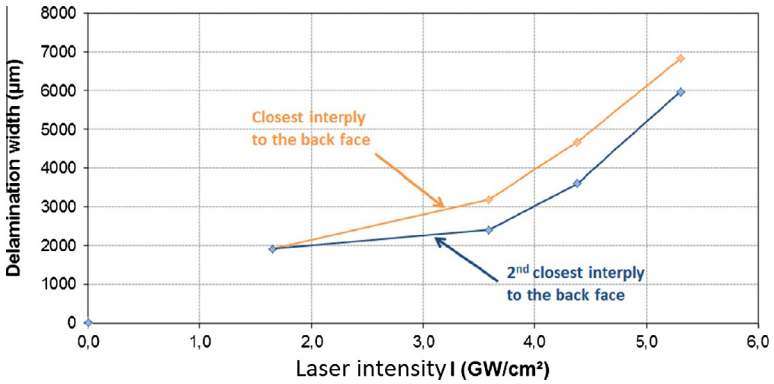

Fig. 5b. Correlation between the laser intensity and the delamination width inside the composite target for two different inter-ply (Results obtained by optical inspection of the same four laser shocks on T800/M21 CFRP target, 1.5 mm thick, presented in Fig. 5a). (For interpretation of the references to color in this figure legend, the reader is referred to the web version of this article).

can locally increase the stress concentration which can explain why the cracks are propagating around these thermoplastic nodules. Finally, the thermoplastic nodules seem to enhance the shock resistance of composite material. Their presence could slow down the crack propagation and thus prevent from an early delamination in case of high intensity impact. This conclusion is also consistent with another work performed to compare the laser shock resistance of a T800/M21 CFRP with a T300/914 CFRP, made with a classic epoxy resin [16].

The observations performed have also highlighted the existing correlation between the laser intensity and the damage extent inside the composite targets. Different damage parameters can be observed thanks to optical micrographies (observations and results presented in Figs. 5a and 5b and 6) and linked to the laser shock parameters. In Fig. 5a, the damage depth is plotted against the laser intensity. The damage depth is representing the distance existing between the sample back face and the furthest observed delamination inside the composite. These measurements have been performed on four different micrographies of an impacted T800/M21 CFRP target also presented in Fig. 5a. It can be noticed that the delamination depth is increasing with the laser intensity. Indeed, the tensile stresses generated by the shock wave propagation are directly linked to the laser energy, meaning the laser intensity if both the focalized diameter and the pulse duration remain constant. The level of stresses is thus higher for higher energy pulse. In case of the lowest laser shock, the tensile stresses, located close to the back face, are just high enough to create a small delamination in the last inter-ply (see in Fig. 5a, first micrography). When the laser intensity is increased, the highest stresses remain located close to the back face, but there is enough energy left propagating backward to delaminate a deepest inter-ply (see in Fig. 5a, second micrography and following ones).

The same kind of correlation can be found between the laser intensity and the delamination width for a given inter-ply (see in Fig. 5b). For highest laser intensity loadings, the tensile stresses initiating the delamination are stronger, which facilitate the damage propagation and finally lead to a wider delamination. The same trend can be observed for several inter-plies. The delamination growth is shifted to higher intensity for the plies located deeper in the composite, which is consistent with the correlation between the laser intensity and the delamination depth.

The crack density evolution has also been studied. Using the micrographies presented in Fig. 5a, the number of transverse cracks inside all the plies was counted over a 10 mm length centered on the laser impact axis for each laser shocks. Consequently, cracks induced by the laser shock wave propagation and cracks resulting from the flexure component of the loading are both taken into account (see Table 1 and Fig. 3). The number of cracks was divided by the 10 mm length to obtain the crack density. As expected, it is increasing with the laser intensity. One more time, the highest laser intensity induces the highest level of damage which agrees with the previous observations.

Finally, all the damage extent parameters seem to increase with the laser intensity. In this case of thin CFRP T800/M21 composite target, a clear correlation is established between the laser intensity irradiating the material and the resulting inside damage. Moreover, a quantification of this correlation has been obtained thanks to these original laser shock results on composite targets.

4.3. Thick CFRP sample measurements

Laser shocks were also performed on the 6 mm thick T800/M21 CFRP samples. Four different laser pulse intensities (similar to the previous ones) have been applied. As this type of samples was much thicker than the previous one, the damage induced by the shock waves propagation inside the material did not spall it completely (compared to the samples presented in Fig. 3). Indeed, the laser shock wave amplitude is more decayed through the material thickness since there is a longer distance to cross before reaching the back face. In this case, the resulting damage is characterized by small blisters on the sample back face, which were measured using Interferometric confocal microscopy and X-ray radiography (see in Fig. 7a–c).

Interferometric confocal microscopy is based on optical interferometry to convert the flux intensity into height information. It is generally used to characterize the surface profile of smallest geometries. In the case presented here, several measurement areas have been needed in order to get the global blister shape. For each pixel located on the back face ply plan by an (x, y) coordinate, a height information is added. The measurement is obtained in the form of a matrix (x, y, z) and can be represented in the plan (x, y) using a color scale for the z coordinate as shown in Fig. 7. In this example, an elliptical shape can be observed. The anisotropic characteristic of the delamination propagation is evidenced by this shape, in spite the axisymmetric loading, but directly linked with the ply orientation. This observation can be confirmed by the X-ray radiography measurement as shown by Fig. 7b and c.

The cross sections of the back face deformation are presented in Fig. 8 and the corresponding ICM measurements are introduced first in Fig. 9. These cross sections were performed perpendicularly to the 0° direction. The two measurement techniques are consistent. Indeed, the delamination width observed in Fig. 8 for each shock is corresponding to the one which can be evaluated in the 0° direction by taking the 0 µm isoheight ICM measurements. The comparisons of the different experimental values are given in Table 2. An accurate study of the ICM experimental results has been performed by using a statistical analysis, considering the experimental data as statistical series. First, it has been checked

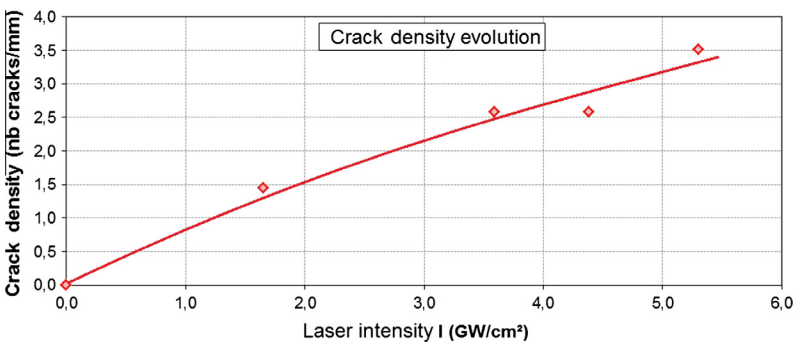

Fig. 6. Correlation between the laser intensity and crack density inside the composite plies (results obtained by optical inspection of four T800/M21 CFRP target shocks, 1.5 mm thick). (For interpretation of the references to color in this figure legend, the reader is referred to the web version of this article).

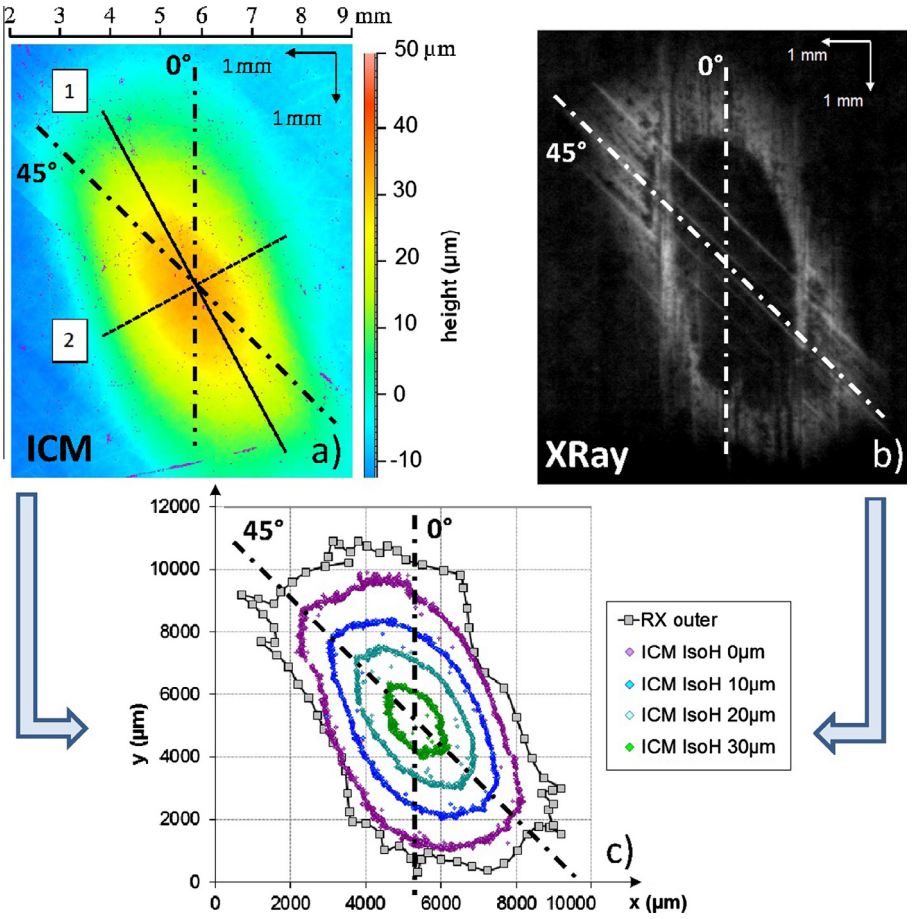

Fig. 7. (a) Interferometric confocal microcopy measurement of a back face deformation resulting from a laser shock on a 6 mm thick T800/M21 composite sample. (b) Corresponding X-ray radiography of the same sample. (c) Comparison between the X-ray radiography measurement and the Interferometric confocal microscopy measurement of the same back face deformation after post-treatment (Water confined laser pulse: $I = 5.30$ GW/cm^2, $\Delta t = 30$ ns, $D_{spot} = 4$ mm). (For interpretation of the references to colour in this figure legend, the reader is referred to the web version of this article.)

that the shape of isoheight is true ellipse. $[x, y]$ data are extracted from the $[x, y, z]$ obtained by ICM, for a given z, meaning a given height. The idea is to show that the correlation between the x and the y data, for all the given heights, is an ellipse. For that, the covariance matrix Σ whose expression is given in Eq. (1) is calculated. The Σ matrix is traducing the correlation between the x and the y data. The main directions of the statistical series x and y are thus given by the eigenvectors of the Σ matrix. For each $[x, y]$ series, the eigenvectors can be calculated using the following equation:

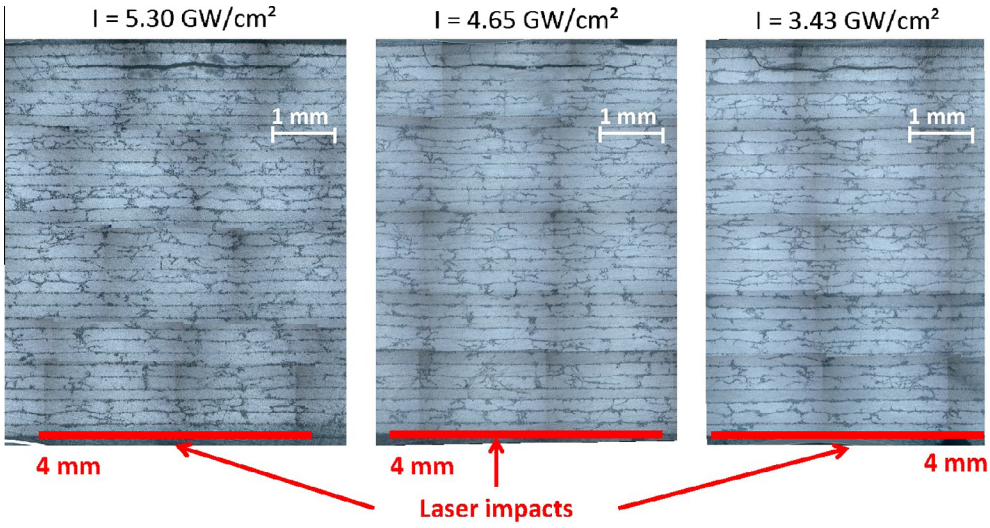

Fig. 8. Cross section micrographies corresponding to the back face deformation measured by ICM and analyzed in the following figures referred 9. (Water confined laser pulse: $\Delta t = 30$ ns, $D_{spot} = 4$ mm). (For interpretation of the references to color in this figure legend, the reader is referred to the web version of this article).

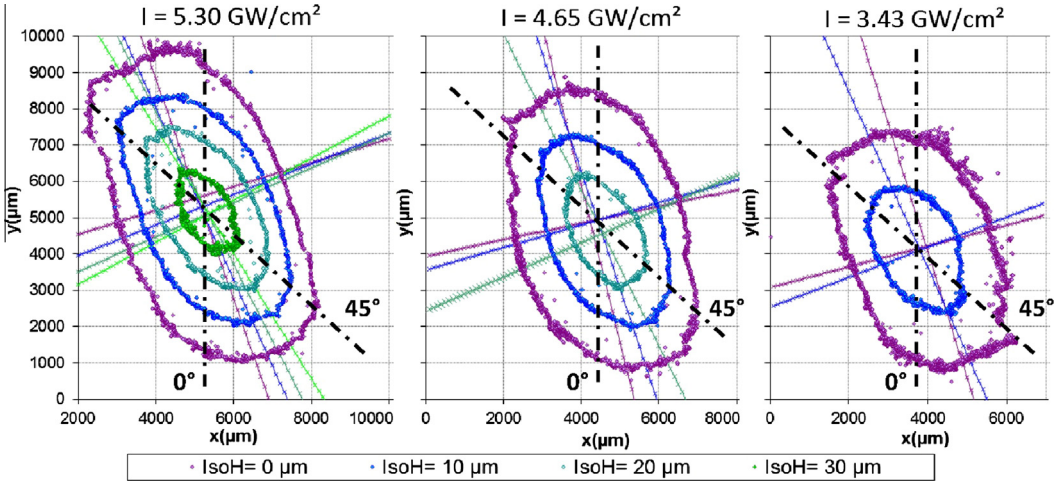

Fig. 9. ICM post treated results for three different laser shock intensities. For different height levels, the (x, y) data highlighting the elliptical back face deformation and the associated major and minor axes calculated by statistical analysis are plotted (water confined laser pulse: Δt = 30 ns, D_{spot} = 4 mm). (For interpretation of the references to color in this figure legend, the reader is referred to the web version of this article).

Table 2
Comparison of the delamination width in the 90° direction measured on micrographies and by ICM.

I (GW/cm²)	Delamination perpendicularly to the 0° direction		
	Micrographies (µm)	ICM (µm)	Deviation (%)
5.30	5095	4713	7.5
4.65	4240	4384	3.4
3.43	3680	3719	1.1

$$\Sigma = \begin{pmatrix} \sigma_x^2 & R\sigma_x\sigma_y \\ R\sigma_x\sigma_y & \sigma_y^2 \end{pmatrix} \quad \text{with} \quad \begin{cases} \sigma_x : \text{standard deviation of the x data} \\ \sigma_y : \text{standard deviation of the y data} \\ \text{R : Correlation coefficient} \end{cases} \tag{1}$$

First, the Eq. (2) is solved for each series to determine their eigenvalues noted λ_1 and λ_2. Once calculated, these eigenvalues can be used to determine the two eigenvectors named U and V of each statistical series using the following equation:

$$Det(\Sigma - \Lambda I) = 0 \quad \text{with} \quad \begin{cases} \Lambda = [\lambda_1, \lambda_2] : \text{vector of eigenvalues} \\ I : \text{Identity matrix of dimension 2} \end{cases} \tag{2}$$

$$\begin{cases} \Sigma \cdot U = \lambda_1 \cdot U \\ \Sigma \cdot V = \lambda_2 \cdot V \end{cases} \quad \text{with} \quad \begin{cases} U : \text{eigenvector associated to } \lambda_1 \\ V : \text{eigenvector associated to } \lambda_2 \end{cases} \tag{3 and 4}$$

As explained previously, the two vectors U and V give the main directions for the statistical series $[x, y]$. It was checked that these vectors were orthogonal for each isoheight series of each laser shock, showing that it could correspond to an elliptical distribution. Then, the two main axes of the statistical $[x, y]$ series can be deduced using the eigenvectors as director vector. A point which is known to be on each axis has to be chosen to plot the axes. In this case, if the two main axes are respectively the minor and the major axes of the ellipse searched, they are passing by the ellipse center. This center point is obtained by calculating the average of all x data as first coordinate, and the average of all y data as second coordinate. All these axes are plotted with their isoheights statistical data $[x, y]$ in Fig. 9. It can be observed that the calculated axes are well corresponding to the major and minor axes of each $[x, y]$ contour lines, and for each laser shock deformation. Finally, the axes got from the eigenvectors can be used to calculate theoretical semi-major and semi-minor axes. The intersection point between the axes and the $[x, y]$ contour line is picked for each series and used to calculate the axes length. Then, the semi-major and semi-minor axes lengths, respectively noted α and β, are used to build the corresponding theoretical elliptical shape with the Eq. (5). For each x value, the corresponding y value is calculated with the parameters α and β using Eq. (5) for each series. The obtained ellipses are then rotated using a classic transformation given in Eq. (6), and translated in the (x, y) plan to be compared to the experimental isoheight data.

$$\frac{x^2}{\alpha^2} + \frac{y^2}{\beta^2} = 1 \quad \text{with} \quad \begin{cases} \alpha : \text{semi-major axis length} \\ \beta : \text{semi-minor axis length} \end{cases} \tag{5}$$

$$z \rightarrow ze^{i\theta} \tag{6}$$

$$S = \pi \cdot \alpha \cdot \beta \tag{7}$$

Some comparisons are given in Fig. 10 for four different isoheight levels measured by ICM on the sample shocked with the highest laser intensity level. The calculated ellipses are fitting quite well with the experimental contour lines. The agreement is even better for the high z values contour-lines, when a few differences can be observed at low height (see z = 0 µm chart in Fig. 10). This is probably due to edges effects which are more significant closer to the back face normal height. Finally, the good agreement between theoretical calculation of the elliptical curves and experimental data enables some model analysis. Three different studies are presented in Figs. 11a, 11b and 11c. The evolution of the semi-major and semi-minor axes lengths with the height level is first presented in Fig. 11a. It can be noticed that for each laser shock both parameters are decreasing when the height level of contour lines is decreasing. The evolutions are linear with a good correlation (see the correlation equations Fig. 11a). It gives precise quantitative data on the blister shape created at the sample back face by the laser shocks. Another interesting parameter is the damage area. It can be calculated using Eq. (7). The evolution of the damage surface area with the height level of the back face deformation is presented in Fig. 11b. Logically, it decreases with the altitude. Curves can be modeled by a quadratic equation as presented in Fig. 11b. Finally, the angles γ_{mi} and γ_{ma} to the horizontal axis of both minor and major axes respectively can be plotted as a function of the back face deformation height. These angles are defined in Fig. 10, on the last chart. Their evolution according to the height deformation for each laser shock are presented in Fig. 11c. A small

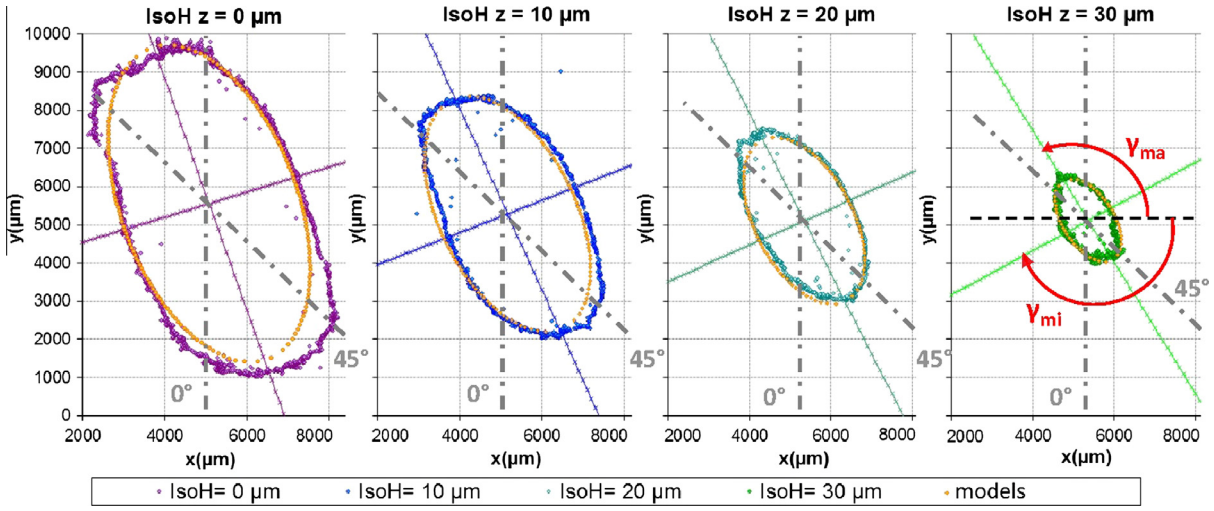

Fig. 10. Comparison between the experimental isoheight lines and the theoretical elliptical shapes calculated using the experimental parameters of the statistical series, for four different isoheight levels measured by ICM on the highest shocked sample. (Water confined laser pulse: I = 5.30 GW/cm^2, Δt = 30 ns, D_{spot} = 4 mm). (For interpretation of the references to color in this figure legend, the reader is referred to the web version of this article).

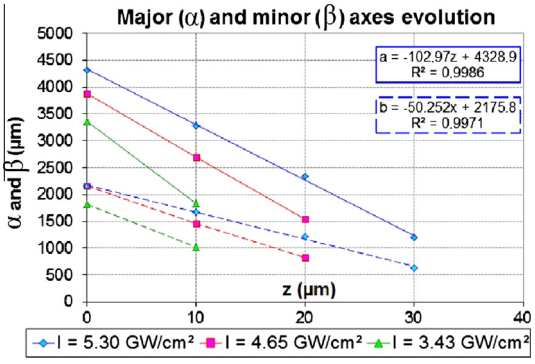

Fig. 11a. Evolution of the semi-minor (dash line) and semi-major axes (plain line) lengths against the height of the contour line with the associated correlations, for the different laser intensities. (For interpretation of the references to color in this figure legend, the reader is referred to the web version of this article).

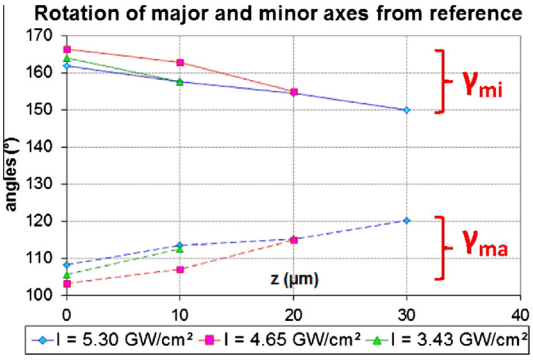

Fig. 11c. Evolution of the angles γ_{ma} and γ_{mi} between the major and minor axes and the horizontal axis against the height of the contour line, for the different laser intensities. (For interpretation of the references to color in this figure legend, the reader is referred to the web version of this article).

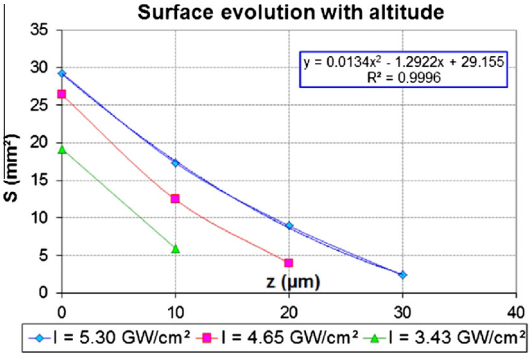

Fig. 11b. Evolution of the in-plane deformation surface defined by the contour line against the height level of the contour line with the associated correlation, for the different laser intensities. (For interpretation of the references to color in this figure legend, the reader is referred to the web version of this article).

rotation of the elliptical contour line of about 15° can be noticed on both axes. This rotation is probably traducing the history of the delamination propagation between the closest plies to the back face. As it can be seen in the Fig. 8, the delamination occurred close to the back face between two 0° plies. The delamination propagated in the 0° direction, but the back face ply is in the +45° direction. This could explain why the deformation orientation at the top of ellipse is closest to the 0° direction than the deformation orientation at the bottom of the blister. Moreover, the bending component of the loading could also have an influence. Once delaminated, the plate bended is non-symmetrical, since it is only composed of two plies in the 0° and 45° directions. The bending of this non-symmetrical plate can increase this unconventional characteristic of the delamination.

This mathematical analysis can then be used to study the existing correlation between the composite back face deformation and the laser intensity. Indeed, by using the major and minor axes deduced from the statistical analysis, blister profiles were extracted from the ICM measurements, especially along these two axes of the elliptical shape (respectively referred 1 and 2 in Fig. 7a). A comparison between these two profiles is given in Fig. 12, which allows quantifying the anisotropy of the back face deformation. These profiles can also be used to correlate the back face deformation with the laser intensity used to irradiate the composite target as shown in Fig. 13. On this figure, the minor and major axes profiles were plotted for the three highest laser shock levels. The back face profile obtained with the lowest one was measured as a completely flat surface, and was not reported on these charts (see laser shock

parameters in Table 3). Two experimental parameters can be gathered on each profile: the maximum height and the width at mid-height, both reported in Table 3. These parameters were used to fit models on the experimental profiles. Indeed, each experimental profile obtained from ICM can be fitted using Gaussian function as presented in Fig. 9, characterized by A, b and c parameters. This kind of function was already used to fit experimental deformation in case of other types of loading on CFPR [31]. The three model parameters corresponding to the optimized fittings are given in Table 3. The "A" parameter is chosen to be equal to the maximum height measured experimentally, and "c" is adjusted to fit the waviness of the deformation profiles. "b" parameter is just used to adjust the position of the symmetrical axis of the model.

The "A" and "c" parameters can then be used to represent the existing correlation between the back face deformation and the laser intensity level. These correlations are presented in Fig. 14. The damage growth, here represented by the maximum height and the waviness parameters, is increasing with the laser intensity level. Moreover, the evolution linking the maximum height to the laser intensity seems to be linear with a good correlation (see in Fig. 14). Thanks to these charts, it can be assumed that the damage threshold on the T800/M21 composite sample tested is close to 2 GW/cm^2. The determination of its exact position would require more laser shock experiments to refine the bottom of the curve and deduce precisely the behavior at low laser intensity. Cross section micrographies have also proved that the inside delamination sizes agree with the back face deformation height (see micrographies in Fig. 8). The lowest shock showing no back face deformation was not delaminated either. The highest back face deformation corresponds to the longer delamination width and so on. These results show that there is a direct link between the inside delamination size and the back face blister height.

Table 3
Experimental and model parameters for the back face deformation profiles.

	Experiments		Models		
I (GW/cm^2)	h_{max} (μm) = A	D (h/2) (μm)	A (μm)	b (μm)	c (μm)
Major axes					
5.30	44.5	6500	44.5	5700	2600
4.65	31.8	5150	31.8	5800	2100
3.43	20.9	4325	20.9	5800	1700
1.83	0	0	0	0	0
Minor axes					
5.30	42.7	3475	42.7	3700	1400
4.65	31.4	2925	31.4	3700	1200
3.43	18.3	2600	18.3	2600	1000
1.83	0	0	0	0	0

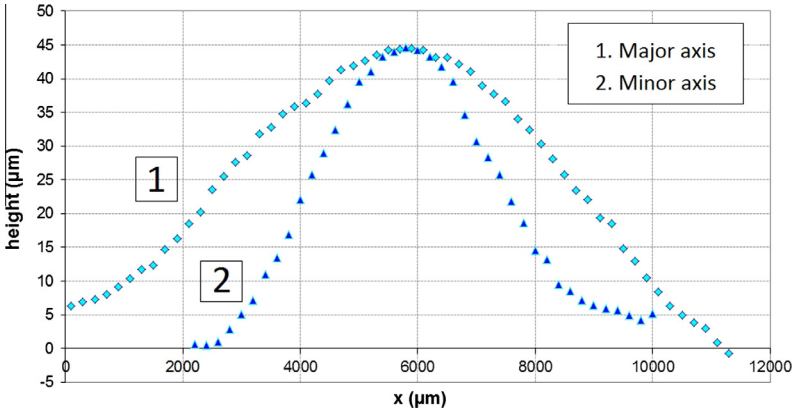

Fig. 12. Comparison between the major and the minor axes of the elliptical back face deformation extracted from the Interferometric confocal microcopy measurement presented in Figs. 7a–c and 9. (Water confined laser pulse: I = 5.30 GW/cm^2, Δt = 30 ns, D_{spot} = 4 mm). (For interpretation of the references to color in this figure legend, the reader is referred to the web version of this article).

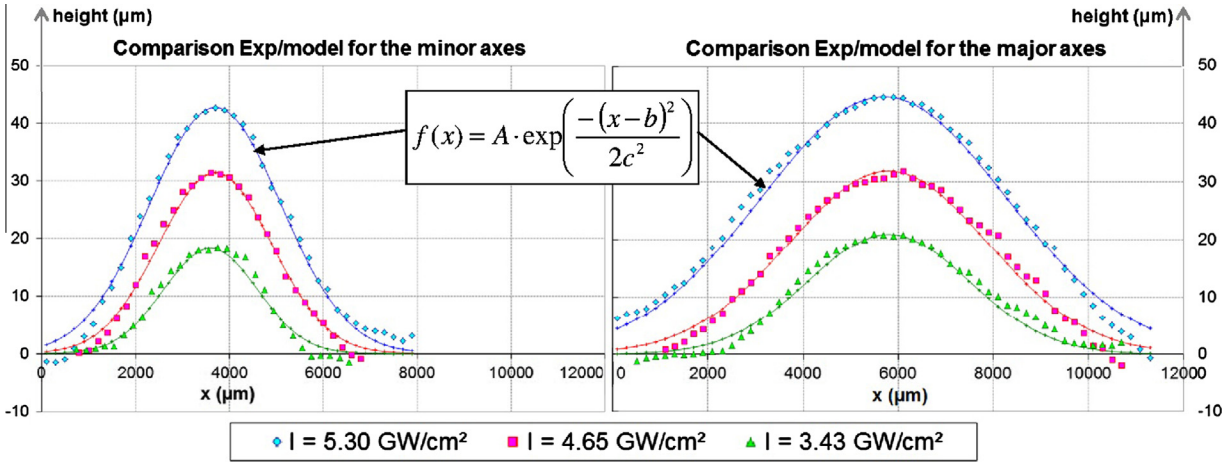

Fig. 13. Comparison between the profiles along the major and the minor axes of the elliptical back face deformation for different laser intensities (water confined laser pulse: Δt = 30 ns, D_{spot} = 4 mm). (For interpretation of the references to color in this figure legend, the reader is referred to the web version of this article).

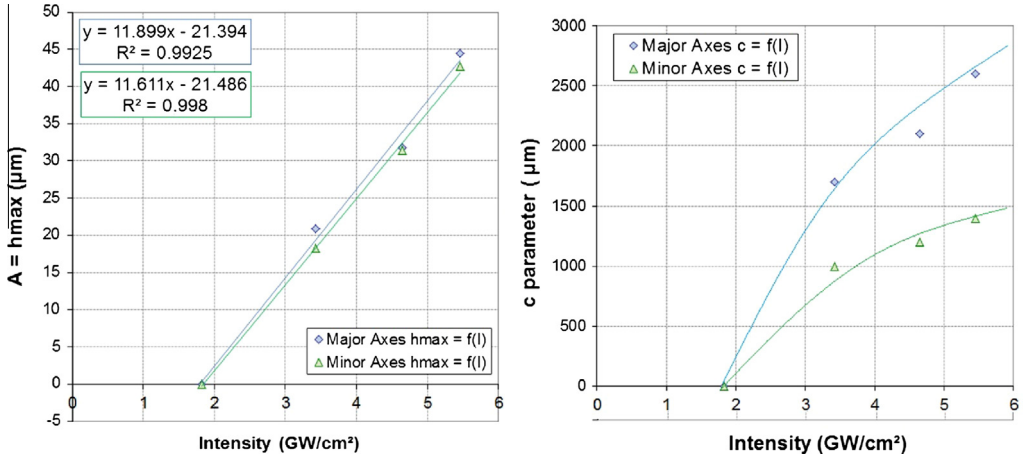

Fig. 14. Correlations between the laser intensity and the main back face deformation parameters (water confined laser pulse: Δt = 30 ns, D_{spot} = 4 mm). (For interpretation of the references to color in this figure legend, the reader is referred to the web version of this article).

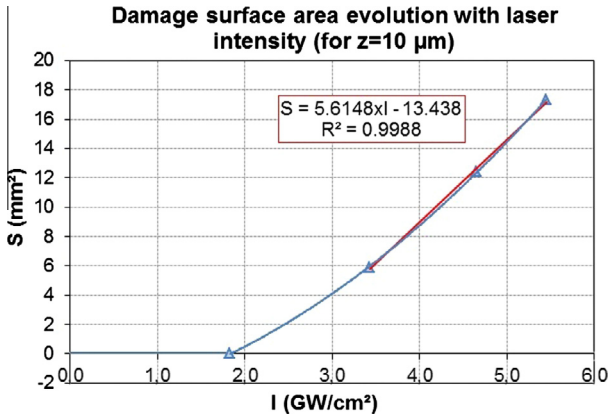

Fig. 15. Evolution of the damage surface area for a given height (z = 10 µm) against the laser intensity, with the associated correlation. Damage threshold determination. (For interpretation of the references to color in this figure legend, the reader is referred to the web version of this article).

Finally, the calculated surface area can also be plotted against the laser intensity for a given height using the α and β length (see Eq. (7)). In the chart presented in Fig. 15, the damage surface area at z = 10 µm is plotted for different laser intensities. The global trend of the obtained curve is quadratic (see the correlation equations in Fig. 15). Fig. 15 also shows that this type of chart provides a good way for the damage threshold determination. The three last correlations between the composite damage features and the laser intensity allow the creation of charts to compare different composite material dynamically loaded. As it has been evaluated in Fig. 14, the damage threshold for the studied T800/M21 composite is confirmed to be around 2 GW/cm^2.

5. Conclusions

The laser shock wave technique has been tested on classical aeronautic composite T800/M21 samples of different thicknesses. This technique results in an intense but really short dynamic loading, which enable the sample recovery for post-mortem analysis. The damage resulting from the laser shock wave propagation inside the material has thus been studied using several diagnostics: optical micrography, X-ray radiographies and Interferometric Confocal Microscopy measurements. The anisotropic damage parameters have been shown as well as the influence of the laser intensity level on the damage main dimensions. A first possible damage scenario for the T800/M21 composite under high laser irradiation was formulated. In particular, the effect of thermoplastic nodules on the cracks propagation is clearly experimentally evidenced. Moreover, the laser shocks performed on thick T800/M21 sample have enabled a better understanding of the dynamic behavior of the composite. More precisely, the resulting back face deformation has been studied using Interferometric confocal microscopy. The relatively new technique has given original data to study the composite damage. The elliptical characteristics of this deformation were determined by use of a statistical analysis of the data gathered. The models established to fit the experimental data provide parameters allowing the correlation between the back face deformation and the laser shock intensity. More investigations remain to be performed before reaching a full comprehension of the composite behavior under high strain rate solicitation. Nevertheless, this original data can be used to plot charts which would enable the comparison of the damage tolerance of different composite material. To this aim, other composite materials can also be studied to compare their dynamic behavior and their shock resistance to the T800/M21 results. All the data gathered provide interesting information for numerical investigations.

Acknowledgments

The team would like to thank all the Pprime staff who contributed to this investigation, especially by helping on the different experimental setups. The research leading to these results has received funding from the European Union's Seventh Framework Program (FP7/2007-2013) under Grant agreement No ACP0-GA-2010-266226 (ENCOMB, Extended Non-Destructive Testing of Composite Bonds).

References

[1] Ehrhart B, Valeske B, Muller C. Methods for the quality assessment of adhesive bonded CFRP structures – a resumé. In: 2nd International Symposium on NDT in, Aerospace; 2010.
[2] Stöven T. Rivetless Aircraft Assembly – A Dream or Feasibility Concept, EUCOMAS, Berlin; 2010.
[3] Catché S, Piquet R, Lachaud F, Castanié B, Bénaben A. Interaction between surface texture after drilling and bearing behaviour of UD carbon/epoxy structures. In: 17ème Journée Nationnales des Composites (JNC). Poitiers, France; June 2011.
[4] Généreux L-A, Viens M, Lebrun G. In: Comparison of ultrasonic testing and infrared thermography for the detection of machining defects in composite materials. In: 26th ASC Annual Technical Conference. Montreal, Canada, September 27th; 2011.

[5] Miyake T, Tanaka T, Ftamura M. Evaluation of machining damage around drilled holes in CFRPs using Micro-Raman spectroscopy. In: 15th European Conference on Composite Materials (ECCM15). Venice, Italy. June 24–28th; 2012.
[6] Ehrhart B, Valeske B, Ecault R, Boustie M, Berthe L, Bockenheimer C. Extended NDT for the quality assessment of adhesive bonded CFRP structures, In: Smart Material, Structures & NDT in Aerospace Conference. Montreal, Canada, November 2–4th; 2011.
[7] Markus S, Tornow C. Extended Non-destructive testing of composite bonds. In: The SAE 2011 Aerotech Congress & Exposition. October 18; 2011.
[8] Vossen JL. Adhesion measurement of thin films, thick film, and bulk coatings. ASTM Spec Tech Publ 1978;1978(640):122–31.
[9] Yuan J, Gupta V. Measurement of interface strength by the modified laser spallation technique. I. Experiment and simulation of the spallation process. J Appl Phys 1993;74:2388–97.
[10] Braccini M, Dupeux M. In: ISTE, Wiley (Eds.), Mechanics of solid interfaces; 2012.
[11] Bossi R, Housen K, Walters CT, Sokol D. Laser bond testing. Mater Eval 2009;67:819–27.
[12] Boustie M, Gay E, Berthe L, Arrigoni M, Radhakrishnan J, de Résséguier T, Blouin A, Monchalin J.P, Kruger S, Perton M, Johnston A, Cole R, Buzaud E. Laser shock adhesion test (LASAT) of composite materials for aerospace industry. In: 23rd Int. Conf. on Surface Modification Technologies (SMT23). Chennai, India. 2–5 Nov; 2009.
[13] Perton M, Blouin A, Monchalin J-P. Adhesive bond testing of carbon–epoxy composites by laser shockwave. J Phys D: Appl Phys 2010;44:034012.
[14] Ecault R, Boustie M, Touchard F, Berthe L, Chocinski-Arnault L, Ehrhart B, Bockenheimer C. Damage of composite materials by use of laser driven shock waves. In: 26th ASC Annual Technical Conference. Montreal, Canada. September 27th; 2011.
[15] Ecault R, Boustie M, Berthe L, Touchard F. Laser Shock Waves: A way to test and damage composite materials for aeronautic applications. In: International High-Power Laser Ablation Conference. Santa Fe, USA. April 30th–May 3rd; 2012.
[16] Ecault R, Boustie M, Berthe L, Touchard F, Ehrhart B, Bockenheimer C. Laser shock wave technique for damage threshold determination of aeronautic composite materials, presented to ECCM15. In: 15th European conference on composite materials. Venice, Italy. 24th–28th June 2012.
[17] Abdallah EA, Bouvet C, Rivallant S, Broll B, Barrau J-J. Experimental analysis of damage creation and permanent indentation on highly oriented plates. Compos Sci Technol 2009;69:1238–45.
[18] Lachaud F, Espinosa C, Michel L. Impact damage of carbone-epoxy laminates. In: 17th JNC Conference. Journée Nationale des Composites. June 15–17th; 2011.
[19] Petit S, Bouvet C, Bergerot A, Barrau J-J. Impact and compression after impact experimental study of a composite laminate with a cork thermal shield. Compos Sci Technol 2007;67:3286–99.
[20] Hongkarnjanakul N, Bouvet C, Rivallant S. The effect of stacking sequence on the low-velocity impact response of composite laminates, ECCM15. In: 15th European conference on composite materials. Venice, Italy. 24th–28th June 2012.
[21] Yen C-F. Ballistic impact modeling of composite materials. In: 7th International LS-DYNA Users conference.
[22] Loikkanen M, Praveen G, Powell D. Simulation of ballistic impact on composite panels. In: 10th International LS-DYNA Users conference.
[23] Craven R, Iannucci L, Olsson R. Delamination buckling: a finite element study woth realistic delamination shapes, multiple delaminations and fibre fracture cracks. Composite Part A 2010;41:684–92.
[24] Schipperen J.H.A. Validation of a progressive failure prediction tool for a dynamically loaded three dimensional composite ship structure, ECCM15. In: 15th European conference on composite materials. Venice, Italy. 24th–28th June 2012.
[25] Yoshimura A, Nagakura K, Okabe T, Kusano H, Yamada M, Tanabe Y, Ogasawara T, Nakatani H, Ogihara S. 3D simulation of high-velocity impact damage progress in the CFRP laminates, ECCM15. In: 15th European conference on composite materials. Venice, Italy. 24th–28th June 2012.
[26] Berthe L, Fabbro R, Peyre P, Tollier L, Bartnicki E. J Appl Phy 1997;82:2826–32.
[27] Gay E 2011 Doctoral thesis (Arts et Métiers ParisTech, France). <http://tel.archives-ouvertes.fr/docs/00/66/75/60/PDF/These_GAY2011.pdf>.
[28] Gay E, Berthe L, Boustie M, Arrigoni M, Mercier P, Bénier J. Experimental study of composite damage under laser shock. In: 17th Journée Nationale des Composite. Poitiers, France; 2011.
[29] Gilath I, Eliezer S, Shkolnik S. J Compos Mat 1990;24:1138–51.
[30] Laporte D, Malaise F, Boustie M, Chevalier J-M, Buzaud E, Thessieux C. Dynamic behaviour of two adhesive materials. In: 18 thDYMAT Technical Meeting, Strasbourg. France 2010.
[31] El-Hajjar RF, Petersen DR. Gaussian function characterization of unnotched tension behavior in a carbon/epoxy composite containing localized fiber waviness. Compos Struct 2011. http://dx.doi.org/10.1016/j.compstruct.2011.03.09.